ORIGINAL ARTICLE

Impact of the Indian part of the summer MJO on West Africa using nudged climate simulations

Elsa Mohino · Serge Janicot · Hervé Douville · Laurent Z. X. Li

Abstract Observational evidence suggests a link between the summer Madden Julian Oscillation (MJO) and anomalous convection over West Africa. This link is further studied with the help of the LMDZ atmospheric general circulation model. The approach is based on nudging the model towards the reanalysis in the Asian monsoon region. The simulation successfully captures the convection associated with the summer MJO in the nudging region. Outside this region the model is free to evolve. Over West Africa it simulates convection anomalies that are similar in magnitude, structure, and timing to the observed ones. In accordance with the observations, the simulation shows that 15–20 days after the maximum increase (decrease) of convection in the Indian Ocean there is a significant reduction (increase) in West African convection. The simulation strongly suggests that in addition to the eastward-moving MJO signal, the westward propagation of a convectively coupled equatorial Rossby wave is needed to explain the overall impact of the MJO on convection over West Africa. These results highlight the use of MJO events to potentially predict regional-scale anomalous convection and rainfall spells over West Africa with a time lag of approximately 15–20 days.

Keywords Madden Julian Oscillation · West Africa · Atmospheric general circulation models · Nudging

E. Mohino (✉)
LOCEAN/IPSL, Université Pierre et Marie Curie,
Tour 45-55, 4eme étage, 4 place Jussieu,
75252 Paris Cedex 05, France
e-mail: emohino@fis.ucm.es

E. Mohino
Universidad de Sevilla, Sevilla, Spain

S. Janicot
LOCEAN/IPSL, IRD, Université Pierre et Marie Curie,
Tour 45-55, 4eme étage, 4 place Jussieu,
75252 Paris Cedex 05, France

H. Douville
Météo-France/CNRM-GAME, Toulouse, France

L. Z. X. Li
LMD/IPSL, CNRS, Université Pierre et Marie Curie,
Paris, France

1 Introduction

Rainfall over West Africa shows great variability with very different periods, including decadal (Giannini et al. 2003; Lu and Delworth 2005; Mohino et al. 2011a), interannual (Rowell et al. 1995; Ward 1998; Giannini et al. 2003; Mohino et al. 2011b) and intraseasonal (Janicot and Sultan 2001; Maloney and Shaman 2008) time scales.

Agricultural production in West Africa depends heavily on intraseasonal rainfall variability (Gadgil and Rao 2000; Sultan et al. 2005). In this time scale, Janicot and Sultan (2001) showed that there are two main periodicities of rainfall and convection over West Africa, with broad peaks in the 10–25 and 25–60 days range. Sultan et al. (2003) showed that the modulation in these two peaks could lead to variations of more than 30% of the seasonal signal. Mounier and Janicot (2004) analysed the 10–25 days range and found evidence of two independent modes of variability, one with a westward propagating signal from eastern Africa to the western tropical Atlantic, and the second one characterized by a stationary uniform modulation of convection in the West African Intertropical Convergence Zone.

The 25–60 days peak shares periodicity range with the Madden-Julian Oscillation (MJO) (Madden and Julian

1994), which is the main mode of tropical intraseasonal variability. Some studies point to a weak or non existent relationship between the MJO and convection over West Africa (Knutson and Weickmann 1987; Maloney and Hartmann 2000). However, Matthews (2004) found that 20 days before enhanced (reduced) convection over West Africa, there was a MJO event with reduced (enhanced) convection over the warm pool. More recent works also support a summer modulation of convection over West Africa by MJO events (Maloney and Shaman 2008; Janicot et al. 2009; Lavender and Matthews 2009; Pohl et al. 2009).

A possible teleconnection mechanism for such modulation was proposed by Matthews (2004), who suggested that dry equatorial eastward Kelvin and westward Rossby waves forced by heating anomalies over the warm pool would propagate around the world and meet over West Africa 20 days later. Maloney and Shaman (2008) results were consistent with upper-level dynamical features related to the propagation of a dry Kelvin wave triggered over the warm pool. However, Janicot et al. (2009, 2010) suggested that a significant contribution came from the Indian region and propagated through westward equatorial convectively coupled Rossby waves. Pohl et al. (2009) also stressed the role of the westward equatorial Rossby waves in propagating the convection signal over West Africa.

Disentangling cause and effect is generally difficult using observations only. General circulation models could help reveal if in fact MJO events impact West Africa and further study the teleconnection mechanism under this impact. Lavender and Matthews (2009) proposed an atmospheric general circulation model experiment in which they forced the model with a SST anomaly associated with the MJO over the Indo-Pacific region. This SST pattern produced convection anomalies over the forcing region that were reminiscent of the ones observed during MJO events. Here we propose a different approach to fully mimic the convection associated with the MJO by assimilating observed data through a so-called nudging or Newtonian relaxation. This technique relaxes some variables of the model towards observed data by adding an extra term to the prognostic equations. It has been used to assimilate data into numerical weather prediction systems and also for the purpose of model validation (Jeuken et al. 1996).

The aim of the work is to study the impact of summer MJO events on convection over West Africa and to further analyse the mechanism for such an impact. We therefore analyse the impact in a simulation nudged over the summer Asian monsoon domain. We use the simulation performed by the LMDZ model guided with reanalysis data in the framework of the IRCAAM project (Influence Réciproque des Climats de l'Afrique de l'Ouest, du sud de l'Asie et du bassin Méditerranéen; Bielli et al. 2010; Douville et al. 2011). The data and methodology used are detailed in Sect.

2. Section 3 studies the observed link between the MJO and anomalous convection over West Africa. The nudged experiment is analysed in Sect. 4. Section 5 is devoted to the study of the teleconnection through the propagation of equatorial waves. The discussion and the main conclusions of the work are given in Sects. 6 and 7, respectively.

2 Data and methodology

2.1 Observations

The daily interpolated NOAA outgoing longwave radiation (OLR) data set (Liebmann and Smith 1996) is used as a proxy of observed convection. It is a globally gridded data set with a spatial resolution of 2.5° × 2.5°. In this work we use May to September data in the period 1979–2008.

For rainfall estimates, version 1.1. of the GPCP 1° daily precipitation data set is used (Huffman et al. 2001). It covers the period 1997-present and it is globally gridded with a spatial resolution of 1°.

To study the dynamics associated with the MJO, reanalysis data from ERA-40 (Uppala et al. 2005) and ERA-Interim (Dee and Uppala 2009) is used. The resolution and time covered by both products are different. The first one covers the period mid-1957 to mid-2002 and the second one 1989-present. In the overlapping period the datasets show differences. For instance, daily zonal winds at 200 and 850 hPa show summer (1 June to 15 September) root mean square differences of 3.3 and 1.3 m/s over the equator (between 15°S and 15°N) in the 1989–2001 period, respectively. However, these differences do not affect our analysis of the MJO: the correlation of the Principal Components (on which our detection of the MJO phase is based, see Sect. 2.3) obtained from ERA40 and ERA-Interim in the overlapping period is 0.997. This high correlation leads to a MJO phase detection that selects the same phase in both data sets in 92% of the cases. The rest of the cases are either due to a threshold value reached in one data set but not in the other one (5% of cases) or to the selection of neighbourhood phases between data sets (3%).

Here we use ERA-40 for the 1979–2000 period and ERA-Interim for the 2001–2008 period. Both products have been interpolated to a common grid of 3° in longitude and 2° in latitude, which is the same as the model's resolution.

2.2 Model and experiments

The LMDZ is a grid-point global atmospheric general circulation model developed in the Institute Pierre et Simon Laplace (IPSL; Hourdin et al. 2006). It is also the atmospheric component of the IPSL ocean–atmosphere coupled

model used in the IPCC-AR4 exercise. In the present study, version 4 is used with a uniform horizontal resolution of 3° in the longitude direction and 2° in the latitude direction. There are 19 layers in the vertical. The LMDZ model has a state-of-the-art physical parameterization, including a prognostic cloud scheme and a complete treatment of surface temperature and hydrology. Each surface grid is furthermore divided into four fractions corresponding to land, open ocean, land ice and sea ice. The planetary boundary layer scheme runs as many times as the sub surfaces to ensure the best treatment of surface turbulent fluxes.

The model runs with SST as lower-boundary conditions and regional nudging in the atmosphere. By nudging, model variables are relaxed to the observed ones. The relaxation is applied by adding at each time step the following term to the prognostic equations:

$$-\frac{\Delta t}{\tau}(x - x_{\text{obs}})$$

where Δt is the time step, x the model's value of the relaxed variable, x_{obs} the observed value towards which the variable is being relaxed (reanalysis data in our case) and τ the relaxation time. This coefficient can be a function of the variable, the location (longitude, latitude and vertical level) and the scale. The relaxation is here applied within a selected domain and is therefore carried out in grid point space. Within the nudging domain τ is horizontally and vertically uniform. Atmospheric temperature (T) and zonal (u) and meridional (v) winds are all relaxed with a relaxation time of half an hour. More details about the grid point nudging technique and its possible use for diagnosing the remote impacts of model errors can be found in Bielli et al. (2010) and Douville et al. (2011). With the nudging technique we force the model to simulate observed phenomena in the desired region. However, the tradeoff is that some budgets might not be balanced anymore in that region.

The experiment consists of 38 boreal summer integrations, one for each individual year from 1971 to 2008 with specified AMIPII (Fiorino 2000) monthly mean climatological SST averaged over the 1971–2000 period. The monthly mean values are daily interpolated before given to the model. The experiment is relaxed in the South Asia and northern Indian Ocean domain (47°E–130°E 15°S–29°N). This domain is centred on the boreal summer Inter-Tropical Convergence Zone. There are 10 realizations of each summer and each realization differs only in the initial conditions. For the nudging, the fields from the 6-hourly ERA40 and ERA-Interim reanalyses are used as a reference for the 1971–2000 and 2001–2008 periods, respectively. Data from the reanalyses is interpolated linearly at the model's time step.

2.3 Methods

2.3.1 Extended empirical orthogonal function (EEOF) analysis

To analyse the MJO cycle, we follow a similar approach as Wheeler and Hendon (2004). We perform EEOF analysis of the zonal wind at 850 and 200 hPa and the OLR standardized anomalies over the whole tropical belt and averaged in latitude between 15°S and 15°N. The fields are previously filtered with a non-recursive filter (Scavuzzo et al. 1998) to extract periodicities in the 20–90 days band. This effectively removes low-frequency variability, in particular interannual variability associated with ENSO (not shown). The conclusions of the work are not sensitive to the actual choice of the filtering band: similar results were obtained with a 30–60 days band. The analysis is applied to the summer (June 1 to September 15) standardized anomalies, unlike Lavender and Matthews (2009), who based their EOF analysis on yearly data. Knutson et al. (1986) argue in favour of separating in seasons when studying the MJO cycle. Further support to this claim is given by the seasonal dependency of the propagation characteristics of the MJO (Knutson et al. 1986; Murakami et al. 1986; Knutson and Weickmann 1987; Wu et al. 2006; Pohl 2007). This is especially true for the summer season, when there is a characteristic northward propagation.

As it will be shown in Sect. 3, the first two EEOFs calculated over the Asian monsoon region can be used to describe the evolution of the summer MJO. To follow this evolution we composite the original fields (previously deseasonalized) in a similar way as Wheeler and Hendon (2004): we represent each day of data as a point in the two-dimensional phase space given by the standardized Principal Components (PC) associated with the first two EE-OFs, PC1 and PC2. Figure 1a shows an example for the year 1996. The sequence starts the first of June, represented in the figure by a square. It shows an anticlockwise rotation around the origin, which means that PC1 leads PC2. This is the general behaviour for all the years. To build the composites we divide the space in the 8 phases defined in Fig. 1b. The dates corresponding to all points that lie in a given phase are used to build the composite for that phase. We disregard any dates with an amplitude below the threshold value of 1.0 standard deviation. The average time between phases is 5 days, which makes a whole cycle of approximately 40 days.

To better compare model and observations, the simulated composites of each phase were built by using the same dates as for the observed ones (Fig. 1b). To test whether a composite average is statistically significant we applied a one-sample t test with the null hypothesis of zero population mean.

Fig. 1 Representation of summer (June 1 to September 15) days as points in the phase space defined by the standardized PC1 (*abscissa*) and PC2 (*ordinate*) obtained from the EEOF on the observed OLR and zonal wind at 850 and 200 hPa: **a** for year 1996; **b** for all years in the 1979–2008 period. The eight phases defined for the composite analysis are also displayed in (**b**)
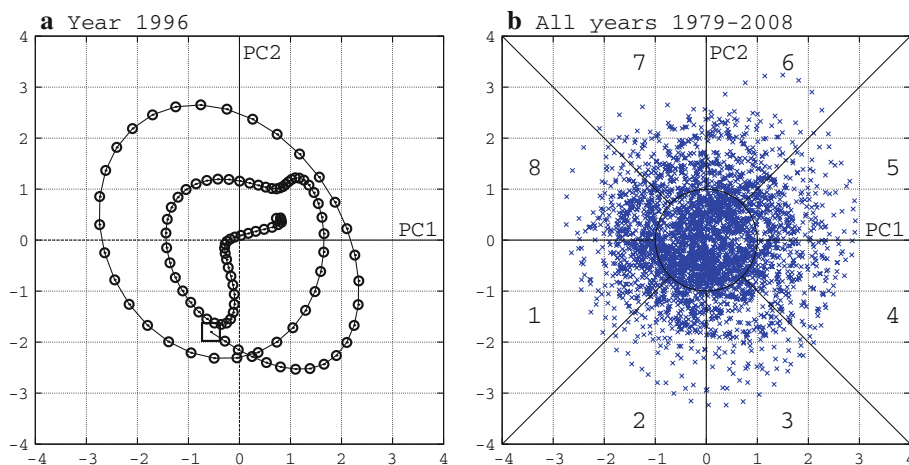
2.3.2 Wavenumber-frequency spectral analysis

To further analyse the equatorial convectively coupled signals, a wavenumber-frequency spectral analysis has been performed on the observed and simulated OLR. This analysis follows a methodology similar to the one used by Wheeler and Kiladis (1999): for each year in the analysis, the summer (1 June—15 September) deseasonalized OLR field between 15°S and 15°N is separated into its symmetric and antisymmetric components with respect to the equator. The mean and trend are removed and the ends are tapered to zero to reduce spectral leakage. A two-dimensional Fourier transform is applied for each latitude and the obtained OLR power is averaged over all years (1979–2008) and summed over all latitudes between 15°S and 15°N. This OLR power is smoothed with a 1–2–1 filter (Von Storch and Zwiers 2001). To highlight the spectral peaks, the obtained OLR power spectrum is divided by a background OLR spectrum. This background spectrum is calculated as in Wheeler and Kiladis (1999): a 1–2–1 filter is applied several times in wavenumber (from five times for small frequencies up to 40 for the highest frequencies) and in frequency (10 times) to the obtained OLR power spectrum.

## 3 Observed evolution of summer MJO and links to convection over West Africa

The spatial structure of the first two EEOFs of OLR and zonal wind at 850 and 200 hPa observed anomalies (previously filtered in the 20–90 days band) is shown in Fig. 2 (black solid lines). These EEOFs explain 28 and 19% of variance in the 20–90 filtered field and are significantly separated from the following ones according to the North et al. (1982) criterion (not shown). The first EEOF depicts a minimum of OLR, i.e. increased convection, over the

Maritime Continent and the West Pacific and two areas of decreased convection centred over the western coast of South America and over central Africa. Meanwhile, the zonal wind anomalies show a baroclinic wave-like behaviour with zonal wavenumber 1. The peak of maximum (minimum) zonal wind anomalies at low (high) levels is located over the Indian Ocean. The corresponding peak of minimum (maximum) anomalies is observed over the eastern Pacific. The second EEOF depicts a minimum of convection over the Indian Ocean. The wind anomalies also show a baroclinic wave-like behaviour but shifted approximately 60° to the east.

These first two EEOFs are not independent. The lead-lag correlation of their associated PCs shows that PC1 leads PC2. The maximum correlation is 0.73 at a lag of 9 days (Fig. 3a). This suggests an eastward propagation of the wind and convection anomalies, associated to the MJO (Madden and Julian 1994). The first two EEOFs are therefore capturing the summer MJO, so their two associated PCs are used to build the composite MJO cycle as explained in Sect. 2.3.

Figure 4 shows the composites of the deseasonalized OLR anomalies for the eight phases defined in Fig. 1b. Over the Indian Ocean and the warm pool, they show the growth and decay of the convective positive and negative phases of the MJO. In phase 1 an anomalous negative OLR anomaly appears in the central equatorial Indian Ocean. The anomaly grows during phase 2, and propagates northward and eastward during phases 3–5, to finally disappear over northern India in phase 6. Over the warm pool, the negative OLR anomalies linger up to phase 7, when they are displaced by the arrival of the positive OLR anomalies associated with the following phase of the summer MJO. The opposite phase of the MJO starts in the central Indian Ocean in phase 5 and follows a similar development with a northward and eastward propagation during phases 6, 7, 8 and 1, and a decay in phases 2 and 3.

Fig. 2 Observed (*black solid line*) and simulated (*grey dashed line*) first two EEOFs of summer OLR and zonal wind at 850 and 200 hPa anomalies (previously filtered in the 20–90 days band): **a** and **b** first and second EEOF of OLR anomalies (units are Wm^{-2} per standard deviation of the associated PC); **c** and **d** first and second EEOF of zonal wind at 850 hPa (units are ms^{-1} per standard deviation of the associated PC); **e** and **f** first and second EEOF of zonal wind at 200 hPa (units are ms^{-1} per standard deviation of the associated PC). *Vertical lines* indicate the longitude interval of the nudging region. *Bottom* plots show the world map between 15°S and 15°N
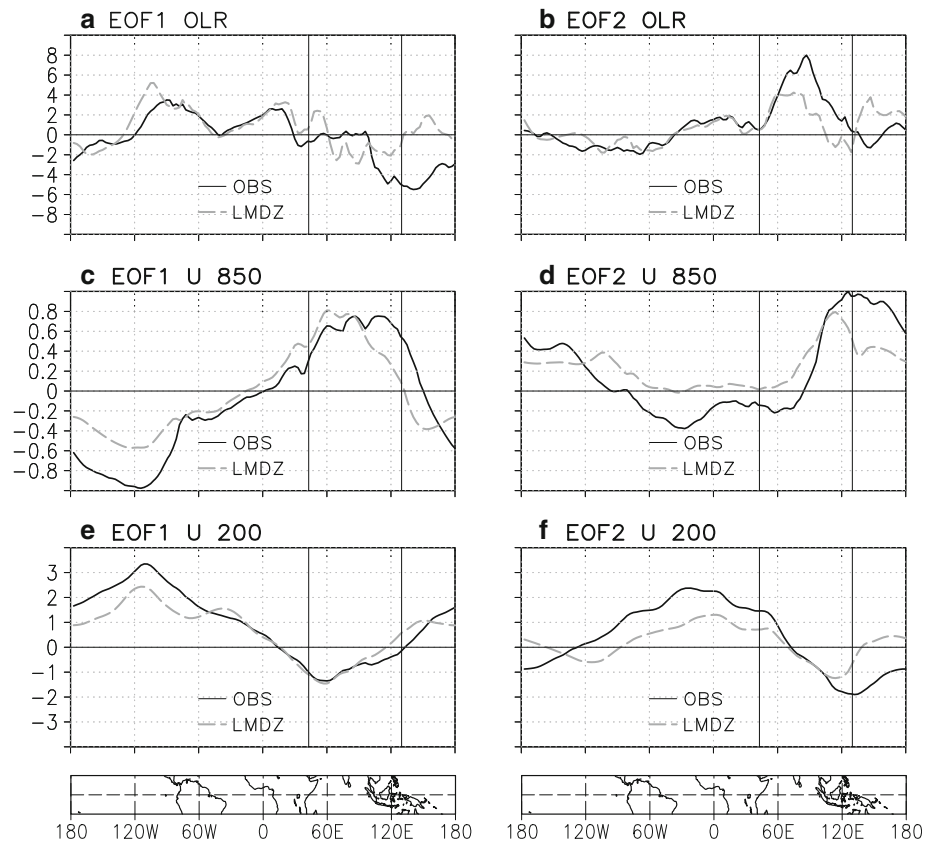
Note that there is a clear northward propagation associated with the summer MJO, in agreement with other studies (Knutson et al. 1986; Murakami et al. 1986; Knutson and Weickmann 1987; Annamalai and Slingo 2001; Wu et al. 2006; Pohl 2007).

Away from the Indian Ocean and the warm pool, the composites in Fig. 4 also show a significant link between the summer MJO and OLR anomalies. Over West Africa (defined hereafter as the region 20°E–20°W and 0–20°N), they show predominantly negative OLR anomalies during phases 8, 1, 2 and 3 and predominantly positive ones during phases 4–7. The maximum negative and positive values are reached at phases 2 and 5, respectively. These maximum negative (positive) values are obtained approximately 15–20 days after the main decrease (increase) of convection over the Indian Ocean. Over West Africa, the OLR anomalies related to the MJO reach 6 Wm^{-2} by phase 2, which represents approximately 130% of the standard deviation of the 20–90 days filtered OLR and 60% of the standard deviation of the whole OLR signal. The impact on precipitation reaches 1 mm/day by phase 2, which represents 240% of the standard deviation of the 20–90 days filtered observed precipitation rainfall (not shown). Over the Sahel (taken as 20°E–20°W and 10°N–20°N), the precipitation shows a mean change between the positive and negative phases of 1 mm/day, which is

approximately 85% of the decadal signal between the 1950s and 1980s (not shown).

The summer MJO displays a clear intra-seasonality. Figure 5a shows that most of the days selected to build the phases associated with the peak of increased convection over the Indian Ocean (phases 2 and 3) tend to happen during the onset of the Indian monsoon in early June, in accordance with Annamalai and Slingo (2001). There is a secondary maximum around mid July, and very reduced activity by the end of the summer. Following the MJO cycle, the phases of decreased convection over the Indian Ocean (phases 6 and 7) tend to happen around 20–30 days after the main increase. This suggests a strong interaction between the active/break cycle of the Indian monsoon and the summer MJO. The MJO also displays interannual variability, alternating years with strong (e.g. 1979, 1996, 2000, 2004–2008) and weak (e.g. 1985, 1990, 1997, 2003) activity (Fig. 5b).

4 Simulation results

4.1 EEOF analysis

Figure 2 (grey dashed lines) shows the first two EEOFs of band-pass filtered (20–90 days) OLR and wind at 850 and

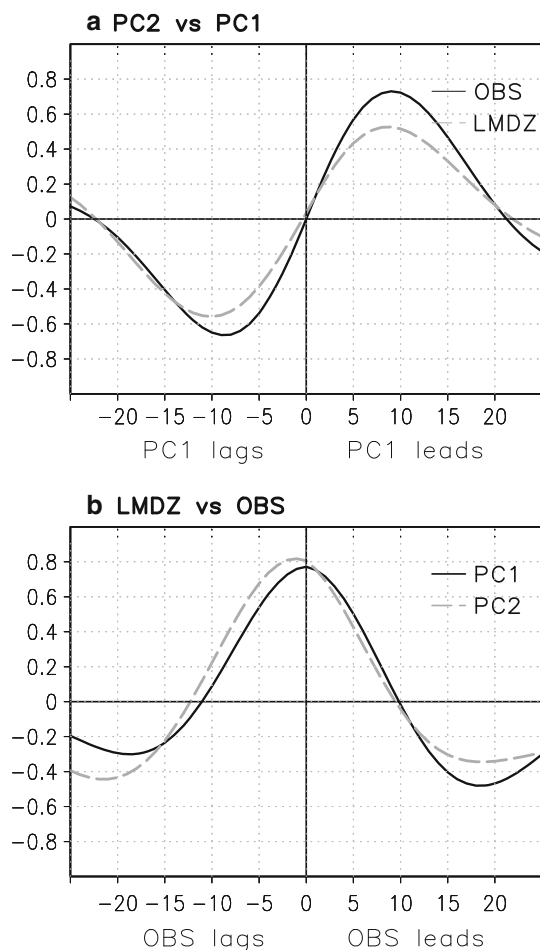## a PC2 vs PC1

b LMDZ vs OBS

Fig. 3 Lead-lag correlations: **a** between the principal components associated with the first and second EEOFs from the observations (*black solid line*) and the model (*grey dashed line*); **b** between the principal components from the observation and the model associated with the first (*black solid line*) and second (*grey dashed line*) EEOFs

200 hPa standardized anomalies from the nudged simulation. The percentage of variance explained by them is lower than in the observations (17 and 9%, respectively). The Principal Components associated with these first two EEOF are significantly separated from the following ones according to the North et al. (1982) criterion (not shown).

The first EEOF of the nudged simulation shows two maxima of OLR centred, like in the observations, over the western coast of South America and over central Africa. Unlike the observations, the anomalies are weak over the warm pool and they show small-scale structures over the nudged region. We will return to this point later in Sect. 4.2. Similarly to the observations, the second EEOF shows a maximum of OLR anomalies in the nudging region. The zonal wind anomalies associated to the two first EEOFs in the simulation show a structure similar to the observed one. In the nudging region, the matching between the simulation and the observations region is better for the zonal wind at

200 hPa. These two EEOFs also suggest an eastward propagation of the anomalies (Fig. 3a). Their corresponding principal components are highly related to the ones obtained from the observations (Fig. 3b).

In the following we use the observed MJO cycle (Fig. 1b) to build the composites for the simulated data. In this way we are able to better compare with the observed composite (Fig. 4).

4.2 Evolution of convection associated with the summer MJO

The composites of the deseasonalized OLR anomalies simulated in the nudged experiment are shown in Fig. 6. Note that they are built using the same dates as the observed ones (Fig. 1b). In the nudged area the OLR anomalies follow a cycle similar to the observed one (Fig. 4): the increased anomalous convection starts in the equatorial Indian Ocean in phase 1 and it grows and propagates northwards to finally decay over the Indian continent in phase 6. Likewise, the decreased anomalous convection begins in phase 5 in the equatorial Indian Ocean, where it migrates northward and decays in phase 1. The simulated OLR response over the nudged region shows less coherency than the observed one, with an increased number of small-scale structures. These could be a side effect induced by the nudging process.

These composite maps shed light into the mismatch shown in the nudged region between simulation and observations in the OLR component of the first EEOF (Fig. 2a). The maximum (minimum) EEOF#1 values take place between phases 4 and 5 (8 and 1; Fig. 1b), when OLR anomalies show a negative (positive) north–south dipole over the Indian Ocean (Figs. 4, 6). In the observations, the averaging between 15°S and 15°N cancels out the anomalies. However, averaging the noisier OLR fields simulated by the model in the nudged region result in small-scale structures in the zonal direction (Fig. 2).

Outside the nudging region, there are differences between the simulated and the observed MJO cycles. The most remarkable one is the lack of a well defined eastward MJO propagation outside the nudging domain. Over West Africa, the simulated composite (Fig. 6) shows a response similar to the observed one (Fig. 4): increased anomalous convection predominates in phases 8 and 1–3, while in phases 4–7 there is mainly decreased anomalous convection. Similarly to the observations, the maximum negative and positive OLR anomalies over West Africa are simulated in phases 2 and 6, respectively. These negative (positive) maximum anomalies occur approximately 15–20 days after the main decrease (increase) of convection over the equatorial Indian Ocean. Over West Africa, the OLR anomalies related to the MJO reach

Fig. 4 Summer composites of observed deseasonalized anomalies of OLR (Wm^{-2}) according to the eight phases defined in Fig. 1b. *Grey* contours mark 95% significant regions (according to a one-sample *t* test)
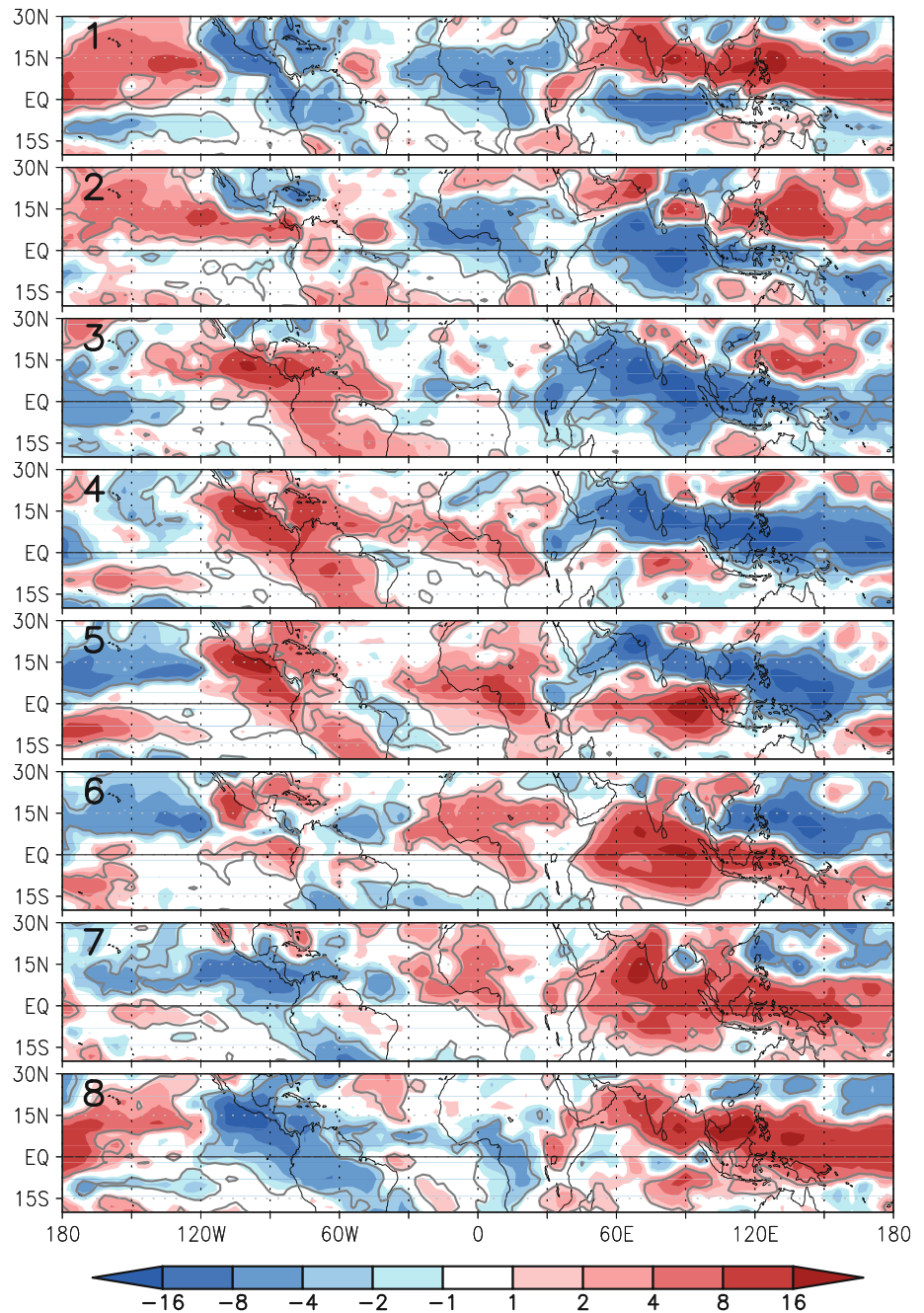
4 Wm^{-2} by phase 2, which is approximately equal to one standard deviation of the 20–90 days filtered OLR. The structure of the OLR anomalies over West Africa and their magnitude are also similar to the observed ones. This result establishes a causal link between the MJO events over the Indian Ocean and the convective anomalies observed later on over West Africa: the model is forced by the convection in the nudged region and is capable of developing a response similar to the observed one over West Africa.

5 Equatorial waves

Matthews (2004) proposed a mechanism to explain the impact of MJO events on West African convection trough the propagation of dry equatorial Kelvin and Rossby waves triggered by the anomalous increased (decreased) convection over the warm pool. According to Gill (1980), an equatorial source of diabatic heating (cooling) can trigger a dry Kelvin wave to the east and a dry equatorial Rossby wave to the west. The dry Kelvin wave is associated with
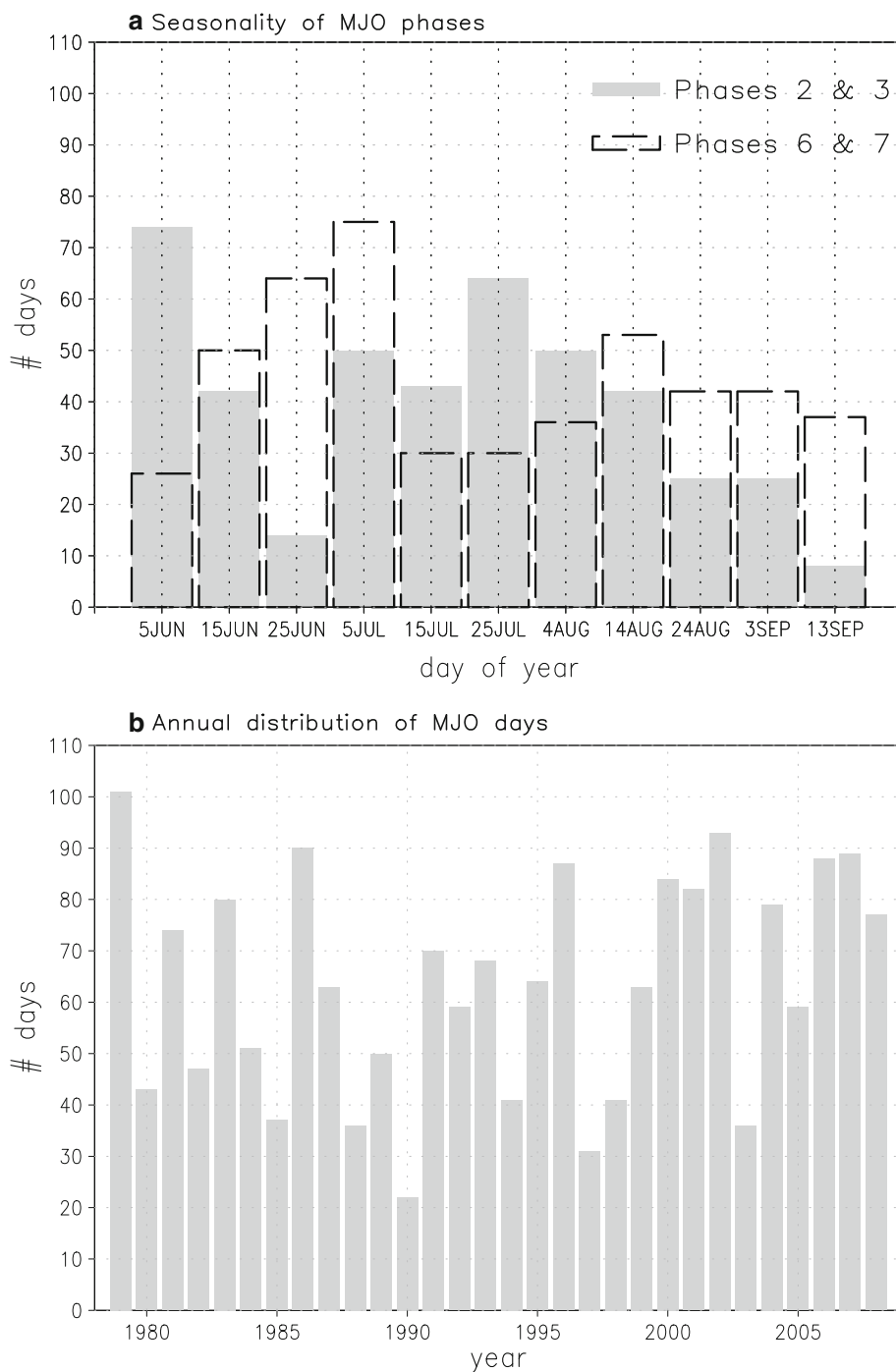
increased (decreased) equatorial tropospheric temperatures, equatorial easterly (westerly) wind anomalies at low levels and descent (ascent) at the wave front. The dry equatorial Rossby wave is associated with a couple of twin cyclones (anticyclones) straddling the equator in low levels, with westerly (easterly) anomalies over the equator and descent (ascent) to the west of the cyclones (anticyclones). Matthews (2004) suggested that these waves would then meet

20 days afterwards over West Africa, where they would favour decreased (increased) convection. In a following work Lavender and Matthews (2009) indicated that the Rossby wave is the most important component with associated westward propagating convective anomalies while the eastward propagating Kelvin wave also triggers convection over the eastern Pacific and central America but less clearly over West Africa.

Fig. 6 Summer composites of deseasonalized OLR anomalies (in Wm^{-2}) simulated by the LMDZ model in the nudged experiment. The composite was built according to the eight phases defined in Fig. 1b. *Grey* contours mark 95% significant regions (according to a one-sample t test). The *box* marks the nudged area
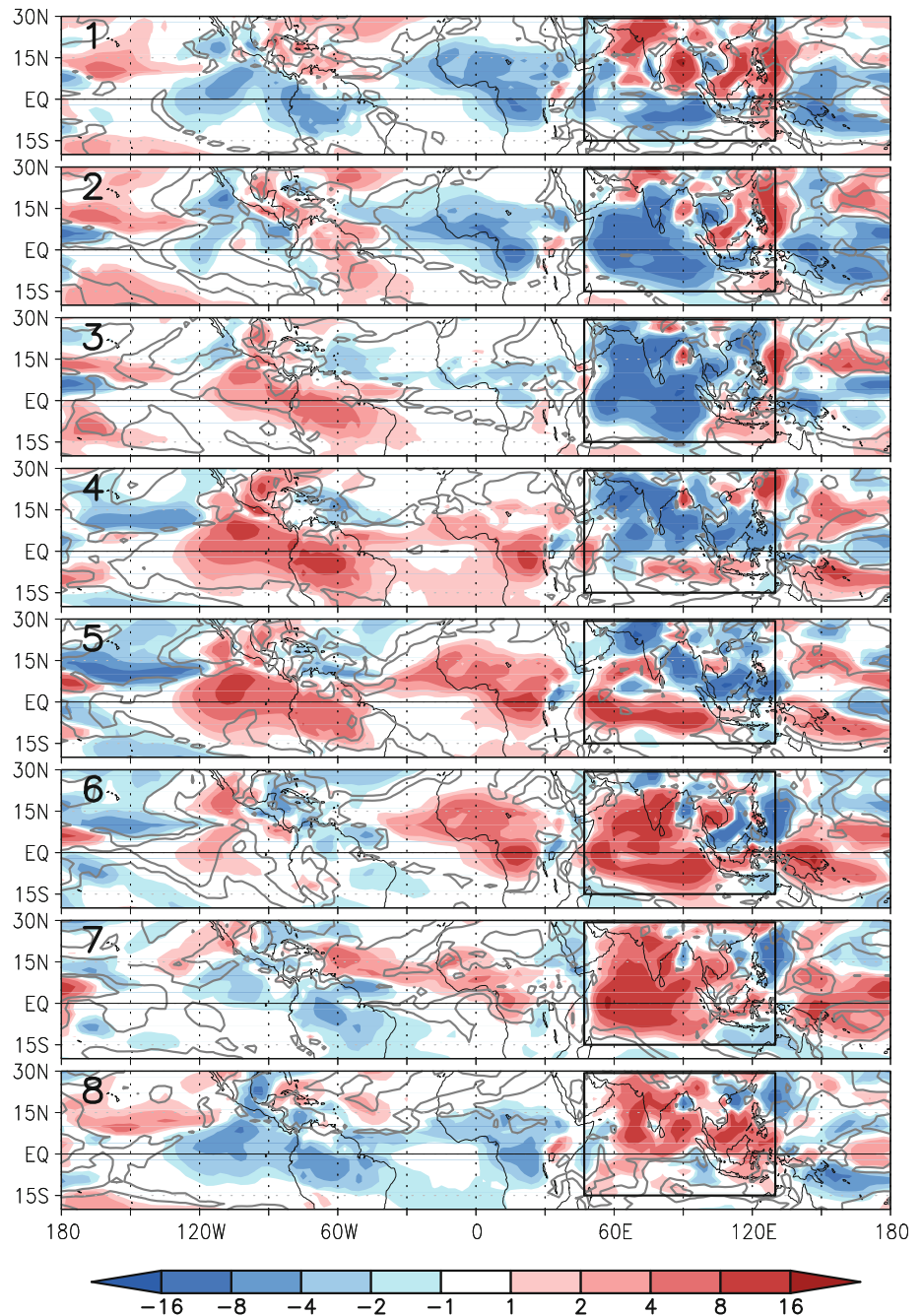

Figure 7 shows the Hovmöller diagram of equatorial (averaged between 10°S and 10°N) deseasonalized anomalies of OLR, temperature at 300 hPa and zonal wind at 850 hPa for the observations and the nudged experiment.

Regarding the observations, the OLR anomalies related to the MJO propagate eastward from the Indian Ocean into the warm pool at a speed of roughly 7 ms^{-1} (Fig. 7a). Warm (cold) temperature anomalies at 300 hPa follow the increased (decreased) convection. Figure 7a shows that once the MJO negative (positive) OLR anomalies weaken (at approximately 160°E), the speed of propagation of the positive (negative) temperature anomalies at 300 hPa changes to about 32 ms^{-1}. This is consistent with a dry equatorial Kelvin wave propagating eastward (Milliff and Madden 1996; Wheeler and Kiladis 1999). The arrival of this wave over West Africa tends to coincide with the occurrence of positive (negative) OLR anomalies, in accordance with the results of Matthews (2004). Similarly, Fig. 7c suggests a dry equatorial Kelvin wave propagating as an easterly (westerly) wind anomaly at low levels. The wind anomalies at 850 hPa propagate approximately 5 days before the 300 hPa temperature ones at a similar
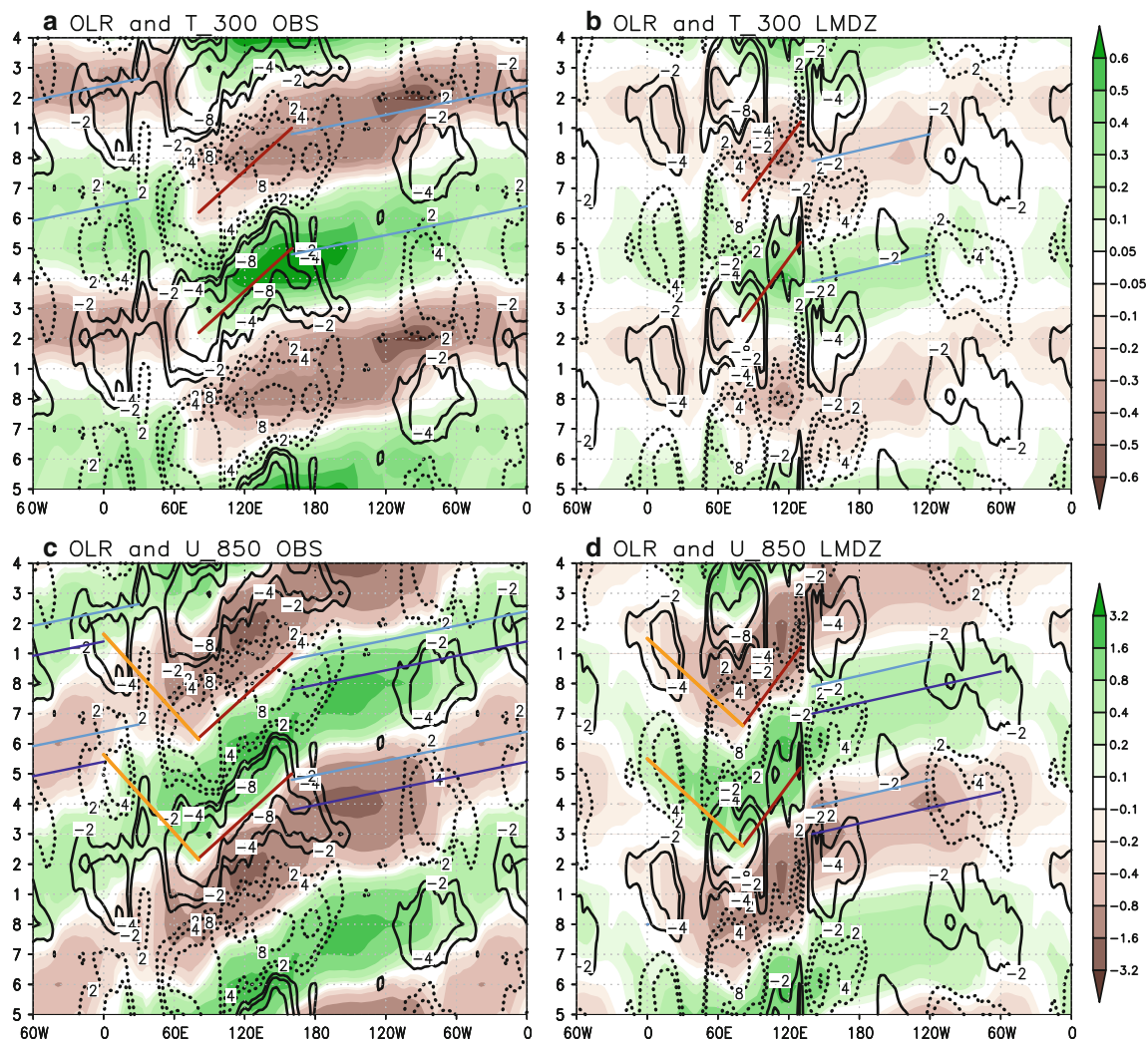
Fig. 7 Composite Hovmöller (longitude vs. phase) diagram of deseasonalized anomalies averaged in latitude between 10°S and 10°N of: **a** observed and **b** simulated tropospheric temperature (in K) at 300 hPa for the observations; **c** observed and **d** simulated zonal wind (in ms^{-1}) at 850 hPa. The *solid* (*dotted*) *black* contours mark OLR (in Wm^{-2}) negative (*positive*) anomalies. The *red line* indicates the eastward propagation of OLR anomalies. The eastward propagation of tropospheric temperature and zonal wind anomalies is indicated by the *light and dark blue lines*, respectively. For easier comparison, the *light blue lines* are repeated in the zonal wind plots. The westward propagation of zonal wind anomalies is indicated by the *orange lines*

speed. In addition, Fig. 7c shows the westward propagation of westerly (easterly) wind anomalies at a speed of approximately 6 ms^{-1}. This is consistent with a convectively coupled equatorial Rossby wave (Wheeler and Kiladis 1999; Yang et al. 2007; Kiladis et al. 2009) rather than a dry equatorial Rossby wave like the ones described by Matthews (2004) or Lavender and Matthews (2009), which showed propagation speeds of 19 and 17 ms^{-1}, respectively. It connects the negative (positive) OLR anomalies over the Indian Ocean with the positive (negative) ones over West Africa, where it coincides with the arrival of the low-level signal of the dry Kelvin wave.

Regarding the simulation, Fig. 7b shows that in the nudging region the OLR anomalies show the eastward propagation of the MJO with approximately the same timing as the observed one. The low level westerly (easterly) winds to the west of the negative (positive) OLR anomalies in the nudged region suggest the westward propagation of a convectively coupled equatorial Rossby wave at a speed of 7 ms^{-1} (Fig. 7d). As in the observations, this convectively coupled equatorial Rossby wave connects the increased (decreased) convection phases of the MJO in the Indian Ocean with decreased (increased) convection over West Africa.

There is also an eastward propagation of high level positive (negative) temperature and low level easterly (westerly) wind anomalies at a speed of roughly 30 ms^{-1}. This suggests a dry Kelvin wave triggered by the MJO phase of increased (decreased) convection in the nudged region. The upper level temperature anomalies associated

with this wave lag the lower level wind anomalies by about 5 days (Fig. 7b, d). The warm (cold) dry equatorial Kelvin wave seems to propagate up to the eastern Pacific and South America, where it coincides with decreased (increased) convection. However, Figs. 7b and d suggest that this simulated dry Kelvin wave does not propagate further east than 60°W, so it would not be related to the anomalous decreased (increased) convection over West Africa centred on phase 5 (1).

Figure 8 shows the wavenumber-frequency spectral analysis of the equatorially symmetric component of observed and simulated OLR. While there is a good correspondence of the MJO and Rossby signals between the observation and the simulation, the model shows very weak power spectra of OLR in the region of the Kelvin wavenumber-frequency theoretical dispersion curves, with no statistically significant peaks, unlike the observations (Fig. 8). Additionally, Fig. 7 shows that the model simulates weaker than observed dry equatorial Kelvin waves. This has been confirmed by computing coherence squared of cross-spectra between the symmetric sea level pressure and temperature at 300 hPa following again Wheeler and Kiladis (1999) procedure (not shown). The simulation, therefore, suggests that the impact of the summer MJO on convection over West Africa is independent of the propagation of both, dry and convectively coupled equatorial Kelvin waves.

To further analyse the different role of the convectively coupled equatorial waves in the relationship shown between the MJO and convection anomalies over West Africa, the composites of OLR anomalies according to the eight phases defined in Fig. 1b are repeated but with filtered OLR in the wavenumber-frequency domain. The filtering is performed through an inverse transform that only retains the Fourier coefficients in the boxes shown in Fig. 8.

Figures 9 and 10 show the composite fields of the MJO-filtered OLR signal, the equatorial Rossby-filtered OLR signal, the MJO and equatorial Rossby -filtered OLR signals and the Kelvin-filtered OLR signal from the observations and the simulation, respectively. The composite sequence of the MJO filtered OLR shows the eastward propagation of observed anomalies all around the world (Fig. 9a). Though less well defined, this propagation is also present in the simulation (Fig. 10a). This signal affects West Africa where it is associated with increased convection in phases 8, 1, 2 and 3 and decreased convection in phases 4, 5, 6 and 7, as in the composite of non-filtered OLR data (Figs. 4, 6). However, the magnitudes are weaker than in the non-filtered data. Figures 9a and 10a also show the characteristic northward propagation of anomalies over the Asian monsoon region related to the summer MJO.
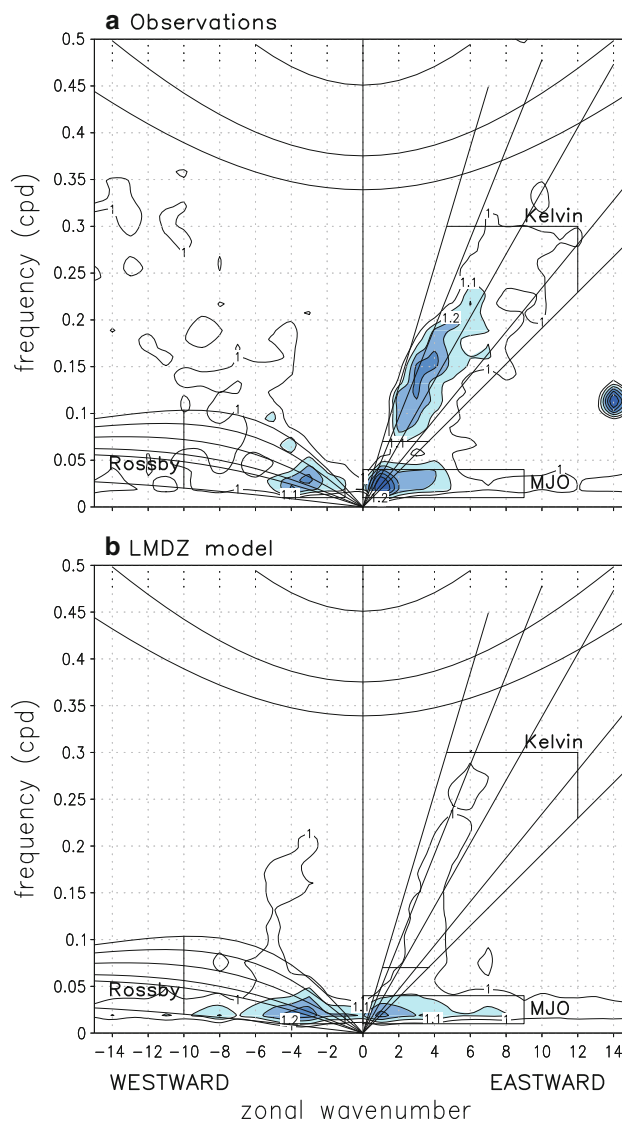

Fig. 8 Wavenumber-frequency spectral analysis of the OLR component symmetric about the equator summed from 15°S to 15°N for 1 June—15 September 1979–2008 for: **a** the observations and **b** the nudged simulation. The spectra is calculated as the ratio of the raw power and the background spectrum (see Wheeler and Kiladis 1999 for details on the computation techniques). Contours intervals start at a ratio of 1.0 and are drawn at an interval of 0.1. The *shading* above the ratio of 1.1 indicates statistically significant signals. The dispersion curves for various equatorial waves are drawn for the equivalent depths of h = 8, 12, 25, 50 and 90 m. An additional dispersion curve for h = 1 m is added for the Equatorial Rossby wave. The *boxes* show the wavenumber-frequency regions used for filtering the MJO, Kelvin and Rossby convective coupled equatorial waves

The equatorial Rossby composites (Figs. 9b, 10b) show that, associated to the MJO, there is also a westward propagating signal that affects convection over West Africa, where it is associated to negative OLR anomalies in phases 8, 1, 2 and 3 and to positive OLR anomalies in phases 4, 5, 6 and 7. The Kelvin-filtered OLR composites
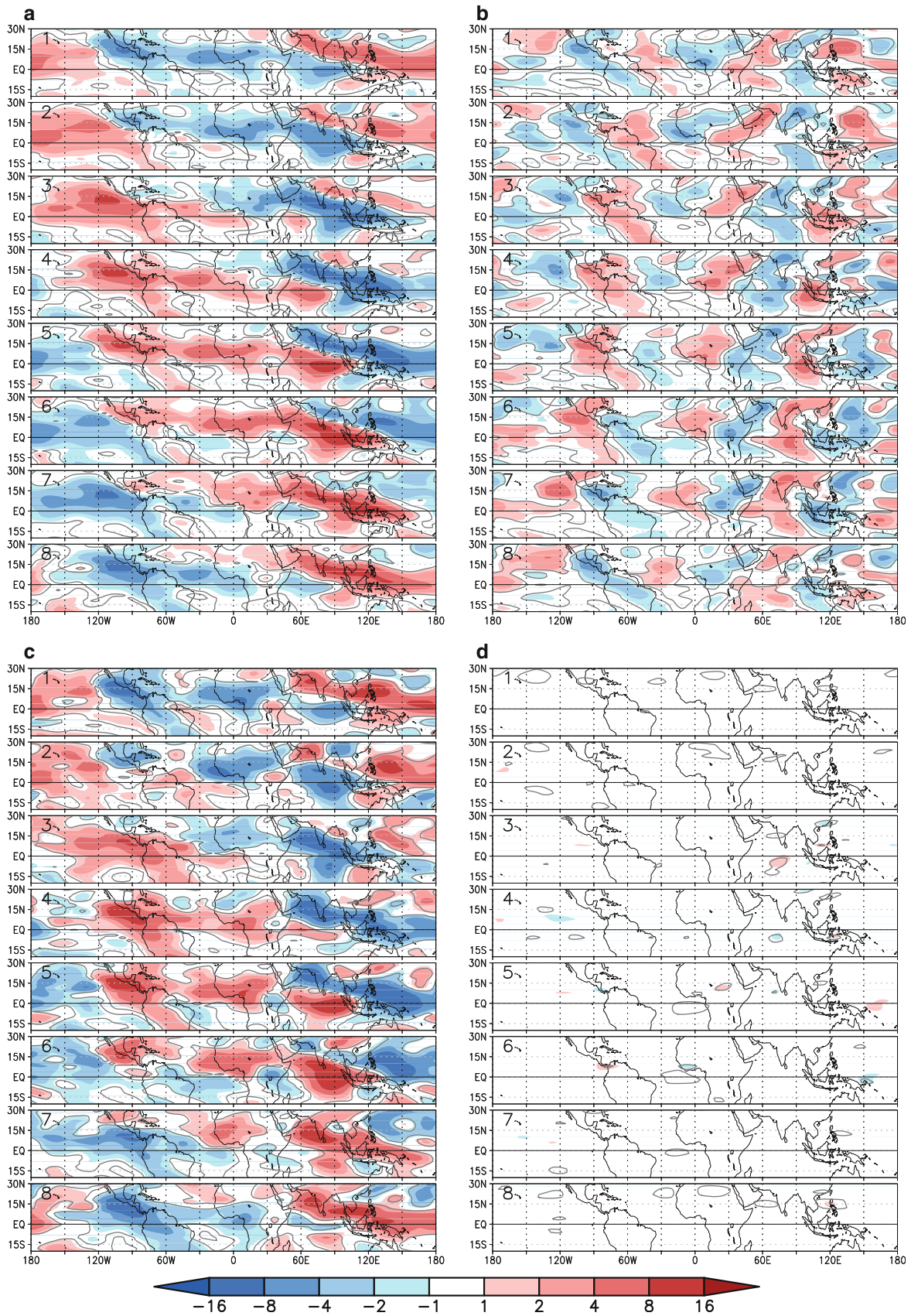
◀ **Fig. 9** Summer composites (according to the phases defined in Fig. 1b) of observed OLR filtered using the *boxes* depicted in Fig. 8 for the: **a** MJO; **b** Rossby; **c** Rossby plus MJO; and **d** Kelvin wavenumber-frequency regions

show a very weak signal (Figs. 9d, 10d), suggesting that the equatorial convectively coupled Kelvin waves have a negligible effect on the relationship between the MJO and West African convection, in agreement with Janicot et al. (2009).

Finally, the composite sequence of the MJO plus equatorial Rossby filtered OLR (Figs. 9c, 10c) shows a pattern very similar to the one obtained with the non-filtered data over the whole tropical belt (Figs. 4, 6). This suggests that in addition to the eastward-moving MJO signal, the westward propagation of convectively coupled equatorial Rossby waves is needed to explain the overall impact of the MJO on convection over West Africa.

6 Discussion

As suggested by Matthews (2004), a possible mechanism to explain the anomalous convection anomalies over West Africa related to the MJO is the change in atmospheric stability due to the mid-tropospheric temperature anomalies associated with the propagation of equatorial waves. However, conversely to the observations, in our experiments the dry Kelvin wave triggered by the MJO events does not seem to reach West Africa. This suggests that the role of this wave is not essential to explain the overall effect of the MJO on convection over West Africa.

A possible explanation for the weak simulated dry Kelvin wave is the area we have used to nudge the simulation, which does not cover the warm pool west of 130°E. Between 130°E and the dateline, the observations show increased (decreased) convection over the equator in phases 3–5 (7, 8 and 1; Fig. 4). This anomalous convection, which is absent in our simulation, is a source of additional diabatic heating (cooling) that contributes to the strength of the dry equatorial Kelvin wave.

Even though our experiments could be underestimating the dry Kelvin wave response to the MJO, the results from the nudged simulation show that the main impact over West Africa can be simulated with the Indian part of the summer MJO.

This study also highlights the potential predictability of regional-scale anomalous convection and rainfall spells over West Africa at intraseasonal time scales. The monitoring of the summer MJO events in the Indian Ocean could provide a prediction of the occurrence of anomalous rainfall over West Africa with an advance of approximately 15–20 days. However, there is a limitation to the real-time prediction due to the strong variability of the MJO events. These events can be highly different from the canonical MJO event obtained from the EEOF analysis (Fig. 2).

In addition, as shown in Sect. 3, the summer MJO cycle shows a clear seasonality, with a high probability of occurrence of increased convection (phases 2 and 3) in the Indian Ocean at the beginning of the Indian Monsoon season (around the 5 June). Hence, the probability of reduced convection over West Africa due to the MJO positive phase peaks approximately 15–20 days after, around the 20–25 June. This date is close to the mean date for the West African monsoon onset (24 June, Sultan and Janicot 2003), which is characterized by a temporary rainfall and convection decrease over West Africa. This could suggest a link between the onset of both monsoons. This issue is addressed in Flaounas et al. (2011).

7 Conclusions

This work presents further evidence that the summer MJO has a clear impact on convection over West Africa. The analysis of the observed OLR shows that approximately 15–20 days after the main positive (negative) convection anomalies over the equatorial Indian Ocean there is reduced (increased) convection over West Africa.

The causal link between the summer MJO and the observed anomalous convection over West Africa has been confirmed with the LMDZ model. To simulate the convection associated with the MJO, the model has been nudged towards the reanalysis data in the Asian monsoon region. Due to this nudging, it shows a cycle of MJO very similar to the observed one in the nudged region. Outside this area, the model is free to evolve. Over West Africa the model develops OLR anomalies that are similar in magnitude, structure, and timing to the observed ones.

The analysis of the observations and the simulation suggest that in addition to the eastward-moving MJO signal, the westward propagation of convectively coupled Rossby waves is needed to explain the overall impact on convection over West Africa. The analysis also suggests that the effect of the convectively coupled Kelvin waves is negligible.

The propagation of the dry Kelvin equatorial wave does not seem to reach West Africa in the nudged experiment. This suggests that the propagation of this wave is not crucial for the impact of the summer MJO on West Africa. The simulation of such a weak Kelvin wave seems to be linked to the area chosen for the nudging, which does not cover the warm pool east of 130°E. However, the model shows that by taking into account only the Indian part of the summer MJO it is able to simulate an impact over West Africa similar to the observed one. This suggests that this is
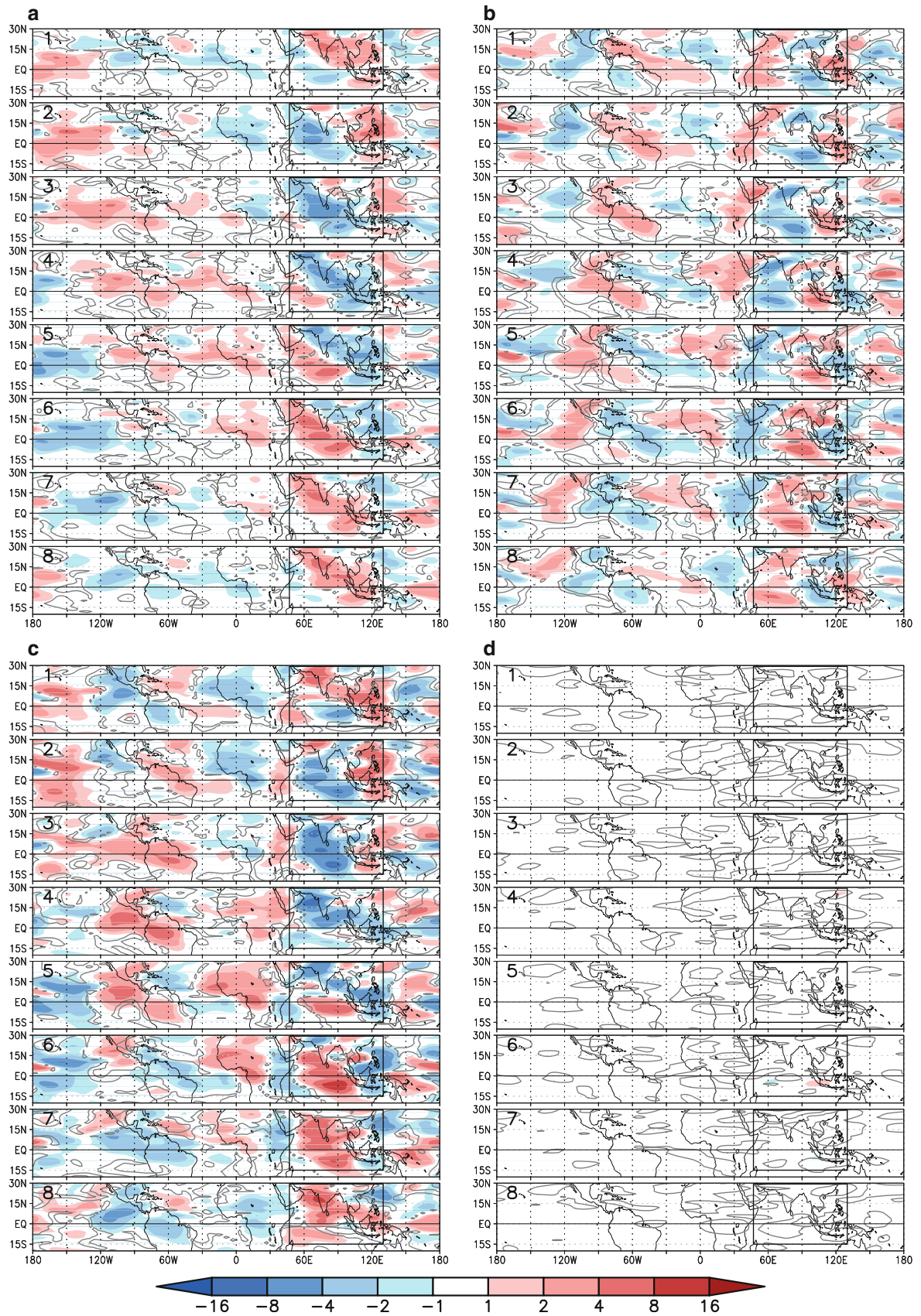
Fig. 10 As in Fig. 9, but for the simulated OLR

a key area for the observed link between the summer MJO and West African convection.

These results also suggest that the observation of a MJO event of enhanced (reduced) convection in the Indian Ocean could be potentially used to predict regional-scale decreased (increased) anomalous convection and rainfall spells over West Africa with a time lag of approximately 15–20 days. The successful simulation of MJO events by some of the latest-generation GCMs could also lead to improvements in the forecast skill of West African intra-seasonal rainfall (Vitart and Molteni 2010; Marshall et al. 2010).

References

Annamalai H, Slingo JM (2001) Active/break cycles; diagnosis of the intraseasonal variability of the Asian summer monsoon. Clim Dyn 18:85–102

Bielli S, Douville H, Pohl B (2010) Understanding the West African monsoon variability and its remote effects: an illustration of the grid point nudging methodology. Clim Dyn 35:159–174. doi:10.1007/s00382-009-0667-8

Dee DP, Uppala S (2009) Variational bias correction of satellite radiance data in the ERA-interim reanalysis. QJR Meteorol Soc 135:1830–1841

Douville H, Bielli S, Cassou C, Déqué M, Hall N, Tyteca S, Voldoire A (2011) Tropical influence on boreal summer mid-latitude stationary waves. Clim Dyn. doi:10.1007/s00382-011-0997-1

Fiorino M (2000) Web document: http://www-pcmdi.llnl.gov/projects/amip/AMIP2EXPDSN/BCS_OBS/amip2_bcs.htm. Last accessed 26 Jan 2011

Flaounas E, Janicot S, Roca R, Li L, Bastin S, Mohino E (2011) The role of dry-air intrusions in the Indian-African monsoon onsets relationship: observations and GCM nudged simulations. Clim Dyn. doi:10.1007/s00382-011-1045-x

Gadgil S, Rao PRS (2000) Farming strategies for a variable climate—a challenge. Curr Sci 78:1203–1215

Giannini A, Saravannan R, Chang P (2003) Oceanic forcing of Sahel rainfall on interannual to interdecadal time scales. Science 302:1027–1030

Gill AE (1980) Some simple solutions for heat-induced tropical circulation. Quart J R Met Soc 106:447–462

Hourdin F, Musat I, Bony S, Braconnot P, Codron F, Dufresne JL, Fairhead L, Filiberti MA, Friedlingstein P, Grandpeix JY, Krinner G, LeVan P, Li ZX, Lott F (2006) The LMDZ4 general circulation model: climate performance and sensitivity to parametrized physics with emphasis on tropical convection. Clim Dyn 27:787–813

Huffman GJ, Adler RF, Morrissey MM, Bolvin DT, Curtis S, Joyce R, McGavock B, Susskind J (2001) Global precipitation at one-degree daily resolution from multisatellite observations. J Hydrometeor 2:36–50

Janicot S, Sultan J (2001) Intra-seasonal modulation of convection in the West African monsoon. Geophys Res Lett 28:523–526

Janicot S, Mounier F, Hall NMJ, Leroux S, Sultan B, Kiladis G (2009) Dynamics of the West African Monsoon. Part IV: analysis of the 25–90-day variability of convection and the role of the Indian Monsoon. J Clim 22:1541–1565

Janicot S, Mounier F, Gervois S, Sultan B, Kiladis G (2010) The dynamics of the West African Monsoon. Part V: the role of convectively coupled equatorial Rossby waves. J Clim 23:4005–4024

Jeuken ABM, Siegmund PC, Heijboer LC (1996) On the potential of assimilating meteorological analyses in a global climate model for the purpose of model validation. J Geophys Res 101:16939–16950

Kiladis GN, Wheeler MC, Haertel PT, Straub KH, Roundy PE (2009) Convectively coupled equatorial waves. Rev Geophys 47:RG2003. doi:10.1029/2008RG000266

Knutson TR, Weickmann KM (1987) 30–60 day atmospheric oscillations: composite life cycles of convection and circulation anomalies. Mon Weather Rev 115:1407–1436

Knutson TR, Weickmann KM, Kutzbach JE (1986) Global-scale intraseasonal oscillations of outgoing longwave radiation and 250 mb zonal wind during Northern Hemisphere summer. Mon Weather Rev 114:605–623

Lavender SL, Matthews AJ (2009) Response of the West African monsoon to the Madden-Julian oscillation. J Clim 22:4097–4116

Liebmann B, Smith C (1996) Description of a complete (interpolated) outgoing longwave radiation dataset. Bull Am Meteorol Soc 106:1275–1277

Lu J, Delworth TL (2005) Oceanic forcing of the late 20th century Sahel drought. Geophys Res Lett 32. doi:10.1029/2005GL023316

Madden RA, Julian PR (1994) Observations of the 40–50 tropical oscillation—a review. Mon Weather Rev 122:814–837

Maloney ED, Hartmann DL (2000) Modulation of eastern North Pacific hurricanes by the Madden-Julian oscillation. J Clim 13:1451–1460

Maloney ED, Shaman J (2008) Intraseasonal variability of the West African monsoon and Atlantic ITCZ. J Clim 21:2898–2918

Marshall AG, Hudson D, Wheeler MC, Hendon HH, Alves O (2010) Assessing the simulation and prediction of rainfall associated with the MJO in the POAMA seasonal forecast system. Clim Dyn. doi:10.1007/s00382-010-0948-2

Matthews A (2004) Intraseasonal variability over the tropical Africa during northern summer. J Clim 17:2427–2440

Milliff RF, Madden RA (1996) The existence and vertical structure of fast, eastward-moving disturbances in the equatorial troposphere. J Atmos Sci 53:586–597

Mohino E, Janicot S, Bader J (2011a) Sahel rainfall and decadal to multi-decadal sea surface temperature variability. Clim Dyn 37:419–440. doi:10.1007/s00382-010-0867-2

Mohino E, Rodriguez-Fonseca B, Mechoso CR, Gervois S, Ruti P, Chauvin F (2011b) Impacts of the tropical Pacific/Indian oceans on the seasonal cycle of the west African monsoon. J Clim 24:3878–3891. doi:10.1175/2011JCLI3988.1

Mounier F, Janicot S (2004) Evidence of two independent modes of convection at intraseasonal timescale in the West African summer monsoon. Geophys Res Lett 31:L16116. doi:10.1029/2004GL020665

Murakami T, Chen LX, Xie A, Shrestha ML (1986) Eastward propagation of 30–60 day perturbations as revealed from outgoing longwave radiation data. J Atmos Sci 43:961–971

North GR, Bell TL, Cahalan RF (1982) Sampling errors in the estimation of empirical orthogonal functions. Mon Weather Rev 110:699–706

Pohl B (2007) L'Oscillation de Madden-Julian et la variabilité pluviométrique régionale en Afrique Subsaharienne. Dissertation, Université de Bourgogne

Pohl B, Janicot S, Fontaine B, Marteau R (2009) Implication of the Madden-Julian oscillation in the 40-day variability of the west African monsoon. J Clim 22:3769–3785

Rowell DP, Folland CK, Maskell K, Ward NM (1995) Variability of summer rainfall over tropical North Africa (1906–92): observations and modelling. Q J Roy Meteor Soc 121:669–704

Scavuzzo CM, Lamfri MA, Teitelbaum H, Lott F (1998) A study of the low-frequency inertio-gravity waves observed during the Pyrénées experiment. J Geophys Res 103(D2):1747–1758

Sultan B, Janicot S (2003) The west African monsoon dynamics. Part II: the "Preonset" and "Onset" of the summer monsoon. J Clim 16:3407–3427

Sultan B, Janicot S, Diedhiou A (2003) The West African monsoon dynamics. Part I: documentation of intraseasonal variability. J Clim 16:3390–3406

Sultan B, Baron C, Dingkuhn M, Sarr B, Janicot S (2005) Agricultural impacts of large-scale variability of the West African monsoon. Agric For Meteorol 128:93–110

Uppala SM et al (2005) The ERA-40 re-analysis. QJR Meteorol Soc 131:2961–3012

Vitart F, Molteni F (2010) Simulation of the Madden-Julian oscillation and its teleconnections in the ECMWF forecast system. Q J R Meteorol Soc 136:842–855

Von Storch H, Zwiers FW (2001) Statistical analysis in climate research. Cambridge Univ Press, Cambridge

Ward MN (1998) Diagnosis and short-lead time prediction of summer rainfall in tropical North Africa at interannual and multidecadal timescales. J Clim 11:3167–3191

Wheeler CM, Hendon HH (2004) An all-season real-time multivariate MJO Index: development of an index for monitoring and prediction. Mon Weather Rev 132:1917–1932

Wheeler M, Kiladis GN (1999) Convectively coupled equatorial waves: analysis of clouds and temperature in the wavenumber-frequency domain. J Atmos Sci 56:374–399

Wu MLC, Schubert SD, Suarez MJ, Pegion PJ (2006) Seasonality and meridional propagation of the MJO. J Clim 19:1901–1921

Yang GY, Hoskins B, Slingo J (2007) Convectively coupled equatorial waves. Part II: propagation characteristics. J Atmos Sci 64:3424–3437